SUPPLEMENTAL MATERIAL

Detailed Methods

Human tissue specimens

Heart specimens were obtained at the time of orthotopic heart transplantation at the Hospital of University of Pennsylvania (for failing hearts) or organ donation (for non-failing hearts) in accordance with the Institutional Review Board approval. Inclusion in tissue-based studies was not restricted on the basis of age, gender, race or ethnic status. Heart failure etiology, body mass index (BMI), age, gender and state of diabetes with respect to dependence on insulin and/or oral hypoglycemic agents of all cases studied here are summarized in the Supplemental Table.

Human heart tissues were divided in pathologically distinct groups as follows. DM-HF represents the group of failing hearts (HF) from patients with overt type-2 diabetes (DM) pre-transplantation (N=25). Both ischemic (ICM) and congestive (DCM) failing hearts were included in the study (Table). With few exceptions, patients in this group were either overweight, i.e. $25 \leq$ BMI <30, (N=7) or obese, i.e. BMI ≥ 30, (N=14), at the date of heart transplant. Some patients in this group were in an advanced stage of diabetes, as they received insulin (N=17). No patient included had a history of ketoacidosis. Other patients in the diabetes group received oral hypoglycemic agents alone (N=6), prior to heart transplant. OW/OB-HF stands for failing hearts from overweight/obese (OW/OB) patients, i.e. BMI ≥ 25, (N=8). Patients in this group presented severely impaired glucose tolerance in response to steroid exposure at the time of heart transplant and developed overt diabetes within 1 year post-transplantation. The OW/OB-NF group (N=8) includes non-failing hearts (NF) from overweight/obese individuals. Heart samples from lean (L), healthy patients without heart failure, i.e. the L-NF group (N=5), and from lean patients with heart failure but no diabetes, i.e. the L-HF group (N=7), served as controls. The L-HF group corresponds to patients with advanced chronic HF of variable duration (range 0.5 to 8 years) and included both individuals with ischemic and nonischemic etiologies for their HF, as shown in Supplemental Table 1.

Experimental Animals

Animal studies were approved by the University of California, Davis Animal Research Committee. Because rodent amylin is not amyloidogenic and rodents do not accumulate amylin amyloids (1), most rodent models are not adequate for this study. We used Sprague-Dawley rats that express human amylin in the pancreatic β-cells on the insulin II promoter (HIP rats) (2). HIP rat breeding pairs were kindly provided by Pfizer. These rats show amylin deposits in pancreatic islets and gradual decline in β-cell mass leading to impaired fasting glucose at 5 months of age and diabetes by 10 months of age (3). As negative controls, we used obese, insulin resistant rats expressing only the native, non-amyloidogenic rat amylin isoform, which does not form amyloids (UCD-T2DM rats) (4-7). The UCD-T2DM rat model was obtained by breading obese Sprague-Dawley rats with Zucker Diabetic Lean rats that have inherent ß-cell defects (4). UCD-T2DM rats exhibit hyperinsulinemia associated with insulin resistance prior to the onset of diabetes (4), similar to HIP rats and humans (2). The model was used for studies of pharmacological and surgical prevention and treatment of type-2 diabetes (5-7). Both HIP and UCD-T2DM rats develop diabetes on a similar time scale, as shown by longitudinal measurements of the pancreatic secretory function reported previously (2-4). In the present study, we used age matched HIP and UCD-T2DM rats in the pre-diabetic state, i.e. *non-fasting* (random) blood glucose level <200 mg/dl. Pre-diabetic male HIP (N=17) and UCD-T2DM

(N=19) rats were used for experiments. Wild-type littermates (N=16) served as non-diabetic controls for HIP rats. Age-matched SD rats (N=13, Charles Rivers Laboratory) were controls for UCD-T2DM rats.

Immunochemistry

Left ventricular tissue was homogenized in homogenization buffer containing 10 mmol/L Tris-HCl, pH 7.4, 150 mmol/L NaCl, 0.1% sodium dodecyl sulfate, 1% TritonX-100, 1% sodium deoxycholate, 5 mmol/L EDTA, 1 mmol/L NaF, 1 mmol/L sodium orthovanadate and protease and phosphatase inhibitor cocktail (Calbiochem). Isolated cardiac mocytes were lysed in lysis buffer containing 1% NP-40, 150 mM NaCl, 10 mM Tris-HCl, 2 mM EGTA, 50 mM NaF and protease and phosphatase inhibitor cocktail (Calbiochem). Blood samples were centrifuged at 3500 rpm to remove cellular components. Human samples were incubated with Protein A-coated magnetic beads (Invitrogen) for 6 hours to remove IgG, a possible source of cross-reactivity. Standard Western blot and dot blot experiments were performed. The following primary antibodies were used: polyclonal anti-amylin antibody (Peninsula) that recognizes both human amylin and rat amylin, polyclonal anti-BNP (Millipore), anti-SERCA monoclonal (clone 2A7-A1 from ABR), monoclonal anti-phospholamban (Badrilla) and polyclonal anti-Na/Ca exchanger (Millipore). For heart samples, equal loading was verified by re-probing with anti-GAPDH. Signal intensity analysis was performed in Image J. For each gel, we averaged the signal intensity of the corresponding bands for the control samples. Then, we normalized the signal intensity in all lanes to this average. This procedure was repeated on at least four gels and for each sample the normalized signal intensity was averaged. In the end, we calculated averages over all the groups used.

Immunohistochemistry was done on thin section from paraffin blocks using the same anti-amylin antibody and biotinylated goat anti-rabbit IgG (Vector) as the secondary antibody.

Cardiac insulin signaling

To determine the insulin responsiveness of the heart, rats were fasted overnight, injected (I.P.) with insulin (10 mU⁄g body weight) or saline, and sacrificed 10 min after injection. Hearts were excised quickly and frozen in liquid nitrogen. Immunoblots were performed on heart homogenates with phospho-Akt-Ser473, total Akt1/2, phospho-GSK3β-Ser9 and total GSK3β (Cell Signaling Danvers, MA). After gel electrophoresis, proteins were transferred on PVDF membranes, blocked and probed with primary antibodies against phospho-Akt-Ser473 or phospho-GSK3β-Ser9. After developing, membranes were stripped and re-probed with antibodies against total Akt and total GSK3β, respectively.

Cardiac myocyte isolation

Rats were anesthetized by I.P. injection of Nembutal (~1 mg/g) and hearts were excised quickly, placed on a Langendorff perfusion apparatus and perfused with 1 mg/ml collagenase (8). When the heart became flaccid, the left ventricular tissue was cut into small pieces, filtered and [Ca] in the cell suspension was progressively increased to 1 mM (8). The standard Tyrode's solution used in these experiments contained (in mM): 140 NaCl, 4 KCl, 1 $MgCl_2$, 10 glucose, 5 HEPES and 1 $CaCl_2$ (pH=7.4). All experiments were done at room temperature (23-25°C).

Intracellular Ca^{2+} measurements

Myocytes were plated on laminin-coated coverslips, mounted on the stage of a fluorescence miscroscope and loaded with Fura-AM or Fluo4-AM (10 μmol/L, for 35 min for both). Fura was alternately excited at 340 (F_{340}) and 380 nm (F_{380}) and emission was collected at 510±20 nm. Fluo-4 was excited at 488 nm and fluorescence collected at 535±30 nm. Data collected with

Fura-2 are expressed as the F_{340}/F_{380} ratio and Fluo4 data are expressed as F/F_0, where F_0 is the fluorescence signal in resting myocytes. Ca^{2+} transients were elicited by stimulation with external electrodes at frequencies between 0.2 and 2 Hz. The passive trans-sarcolemmal Ca^{2+} leak was measured as the initial rate of $[Ca^{2+}]_i$ declines upon reducing external Ca^{2+} from 1 to 0 mM. Ca^{2+} fluxes to and from the SR were blocked by pre-treating the cells with 10 μM thapsigargin for 10 min whereas the Na/Ca exchanger and sarcolemmal Ca^{2+}-ATPase were abolished by using $0Na^+/0Ca^+$ solution (Na^+ replaced with Li^+) and adding 20 μM carboxyeosin, respectively.

Activation of Ca^{2+}-dependent hypertrophic pathways

Activation of Ca^{2+}/calmodulin-dependent protein kinase II-histone deacetylase (HDAC) and calcineurin- nuclear factor of activated T cells (NFAT) hypertrophic pathways was examined by determining the nuclear *vs*. cytosolic localization of HDAC4 and NFATc4 in cardiac myocytes. Cells freshly isolated from pre-diabetic HIP and age-matched WT rats were plated on laminin-coated coveslips, fixed with paraformaldehyde, permeabilized with 0.2% Triton-100, blocked with 2% goat serum and labeled with polyclonal primary antibodies against HDAC4 and NFATc4 (Santa Cruz Biotechnology). Anti-rabbit Alexa Fluor 488 was used as secondary antibody and fluorescence images were collected with a laser scanning confocal microscope. The ratio of the average fluorescence signal in the nucleus *vs.* cytosol was calculated with Image J.

***In vivo* echocardiography and hemodynamics**

The rats were anesthetized with 50 mg/kg ketamine and 5 mg/kg xylazine, their chests were shaved, and an echocardiogram was done (Acuson, Sequoia model C512, 15-MHz probe) (9). Two-dimensional imaging was used to identify the short-axis position. Three consecutive m-mode images were collected in the short-axis view and saved for analysis of chamber size and fractional shortening. In an animal subset, while the rat was under anesthesia, a carotid artery catheter was passed into the left ventricle to assess pressure/volume loops (9). Fractional shortening, heart rate, ventricular pressure, cardiac output, dP/dt, stroke work and pressure/volume loops were measured.

Electron microscopy

To visualize the nature of the molecular entities formed by human and rat amylin at 50μM peptide concentration in serum, aliquots of each aggregation reaction were imaged by a Philips CM 12 electron microscope (10). The aliquots were deposited onto freshly glow-discharged carbon films. The carbon films were supported by lacy Formvar/carbon films on 200-mesh copper grids. Small sample drops were allowed to sit for 2 min on the carbon surfaces, and then excess fluid was blotted away. The carbon surfaces were then rinsed by applying 5-μL drops of deionized water for 1 min to remove the buffer. Finally, the samples were negatively stained by applying 5 μL of 1% uranyl acetate for 1 min. Electron microscopy images were recorded at 26,000× magnification.

Statistical Analysis

Data are expressed as mean ± SEM. Statistical discriminations were performed using two-tailed unpaired Student's t test, with $P < 0.05$ considered significant. One way analysis of variance (ANOVA) with the Dunnett post hoc test was used when comparing multiple groups.

Online Figure I.
Negative control experiments aimed at testing the specificity of the bands identified in Western blot analysis in Fig 1. Duplicate samples were loaded onto a gel and after blotting and blocking, the membrane was cut and one half was incubated with the anti-amylin antibody while the other half was incubated in the absence of a primary antibody. Both halves were then incubated with the secondary antibody and developed and imaged together. The supplemental figure shows that there is no cross-reactivity with the secondary antibody.

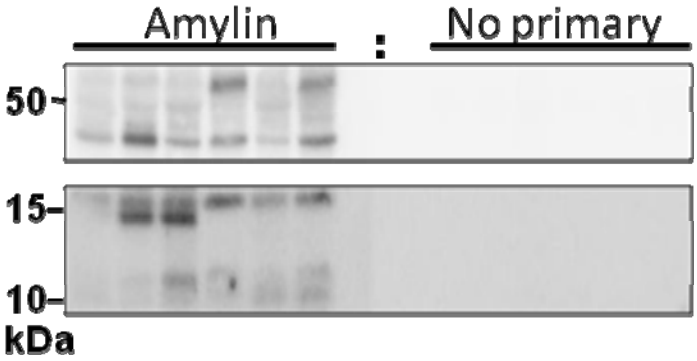

Online Figure II

To estimate the amylin content in insoluble fractions from human heart protein homogenates, pellets were treated with formic acid, freeze dried and then the resulting powders were re-suspended in guanidine hydrochloride. Dot blots with an anti-amylin antibody (**A**) showed significantly increased amylin levels in post-treatment versus pre-treatment samples (**B**). (P = 0.02, Student's t-test.) The test suggests that large amylin aggregates fragmented into small oligomers that were recognized by the anti-amylin antibody.

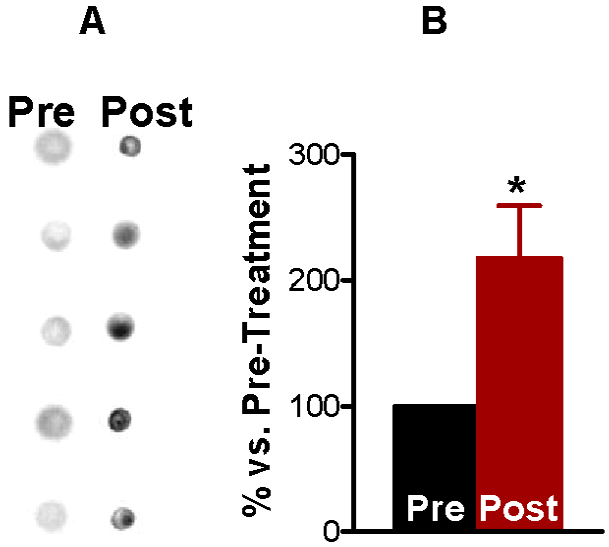

Online Figure III

Electron microscopy of amylin oligomer formation in serum. Electron microscopy images show that 50 µM *human* amylin incubated in serum for 1h has a faster oligomerization reaction than *rat* amylin and forms oligomers and protofibrils (arrow). Oligomerization of *human* amylin resulted in a marked rise in Ca^{2+} transient amplitude (see Fig.3).

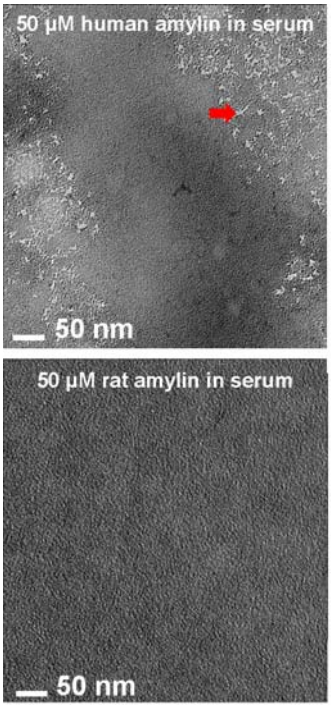

Online Figure IV

Ca^{2+} transient decay (A) and diastolic $[Ca^{2+}]_i$ (B) in control rat myocytes (Ctl) and myocytes pre-incubated for 1-2 hours with 50 μM human (h-amylin) or rat amylin (r-amylin).

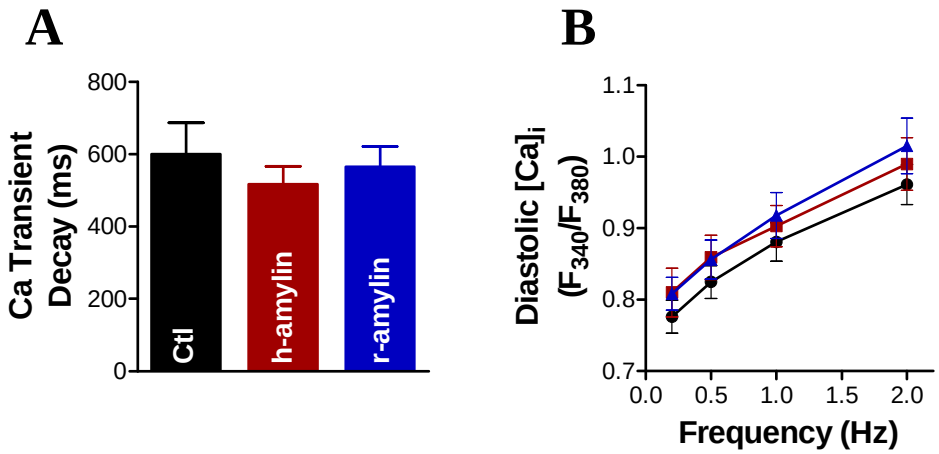

Online Figure V

Human amylin attaches to cardiac myocyte sarcolemma.

(A) Isolated rat myocytes were incubated with 50 µmol/L human amylin (+) or with PBS (–) for 2 h at room temperature. Myocytes were then washed with PBS, lysed and immunoblots were performed with an anti-amylin antibody. The results show the presence of human amylin monomers, dimers and trimers in the group treated with human amylin. (B) Isolated rat myocytes were plated on glass coverslips and incubated with 20 µmol/L of fluorescent FAM-human amylin (AnaSpec) for 2 h. Myocytes were then washed and confocal fluorescence images were recorded. Data show fluorescence staining of the sarcolemma, indicating that human amylin binds to the myocyte membrane.

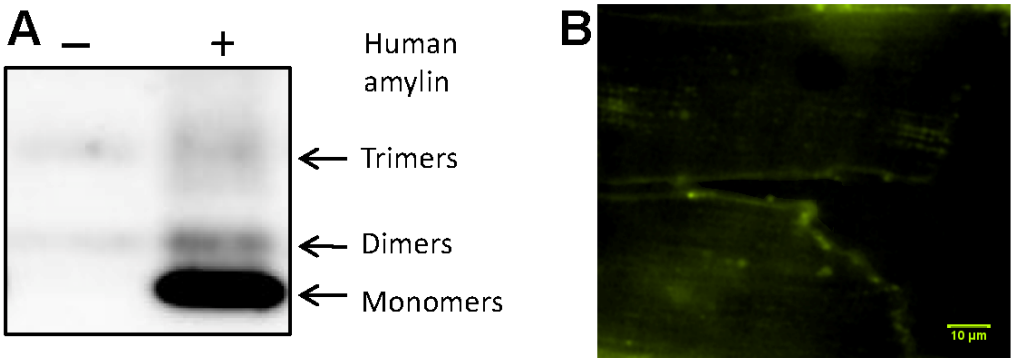

Online Figure VI

GSK-3β phosphorylation in hearts from pre-diabetic HIP and UCD-T2DM rats and littermate controls under basal conditions (0 insulin) and following stimulation with insulin (10 mU⁄g body weight). Representative example and mean values for the ratio between phosphorylated and total GSK-3β. N=3 rats for each group.

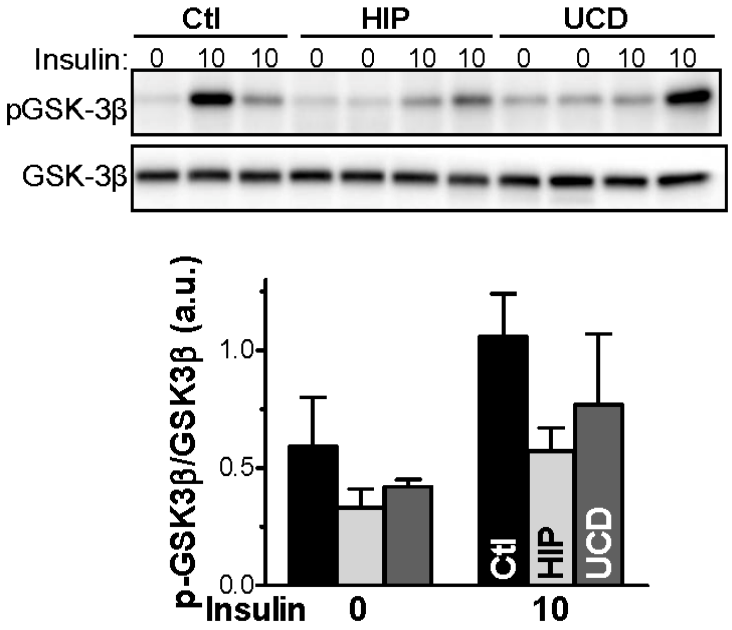

Online Figure VII
Representative Ca^{2+} transients in myocytes from control (Ctl) and pre-diabetic (PD) UCD-T2DM rats paced at 0.5 Hz and 2 Hz.

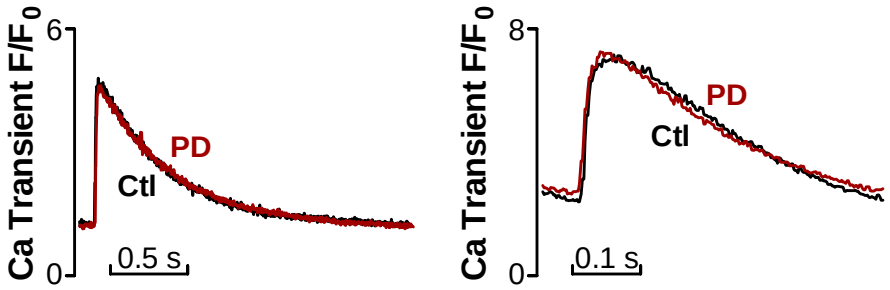

Online Figure VIII

Nuclear import of NFAT and unchanged HDAC distribution in rat myocytes incubated with 50 µmol/L human amylin for 2 h.

The top panels show representative images from control myocytes (untreated) and cells incubated with human amylin (H-amylin). The bottom panels show the quantification of the nuclear-to-cytosolic ratio for HDAC4 and NFATc4. Experiments were done on more than 12 cells for each group.

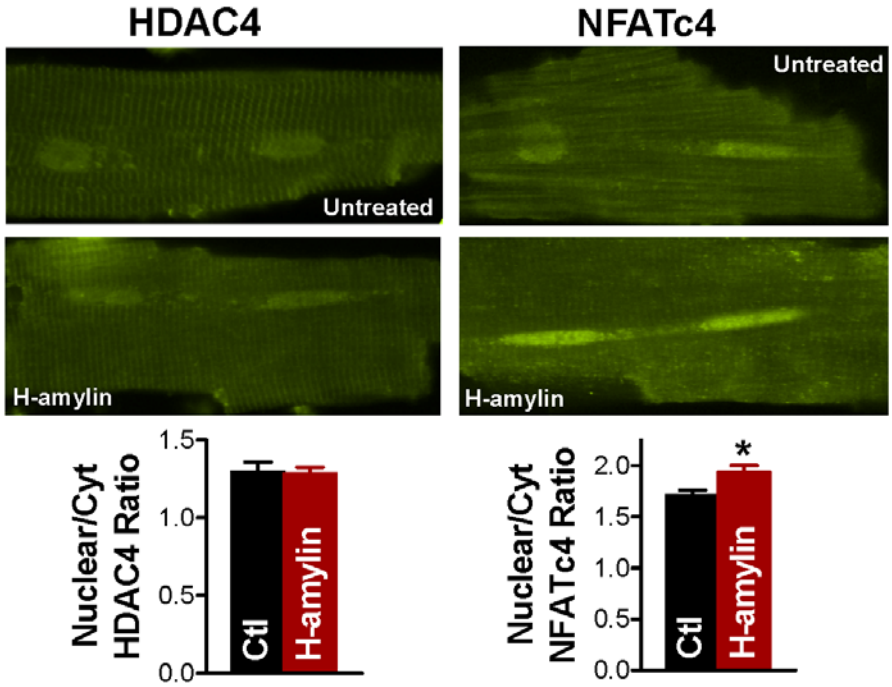

Online Figure IX

BNP and SERCA levels in hearts from UCD-T2DM rats.

(A) BNP level is elevated in hearts from diabetic but not in pre-diabetic UCD-T2DM rats. (B) SERCA expression is unchanged in hearts from pre-diabetic UCD-T2DM rats. Ctl – 5 hearts; PD – 5 hearts, DM – 5 hearts**.**

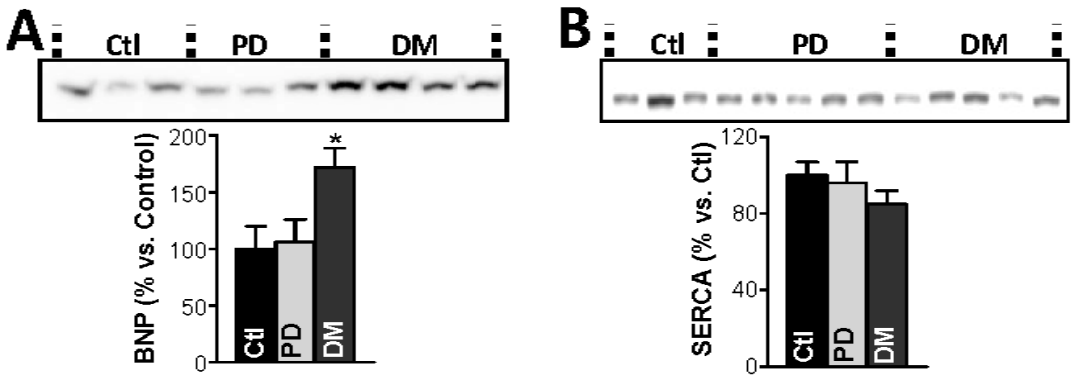

Online Table I. Heart failure etiology, gender, age, BMI, and state of diabetes with respect to hyperglycemia and dependence of insulin and/or hypoglycemics for all patients from who heart tissue was used in this study.

Code	HF Etiology	Gender	Age	BMI
DM-HF (Insulin)	ICM	M	50	32
			58	25.7
			59	31.4
			64	36.6
			58	25.7
	DCM	F	61	28
			44	31.2
			43	40.3
		M	45	32.2
			54	28.6
			64	25.5
			59	27.7
			67	31.2
			56	32.1
			47	35.2
DM-HF (Hypoglycemics)	ICM	M	60	35
			66	20.6
			56	31
			60	20.6
			63	24.3
	DCM	M	38	32.1
			58	34
			66	23.1
			58	34
		F	58	28.4
OW/OB-HF	ICM	M	42	28
			58	22.7
			63	25.2
			54	23.8
			47	25.9
			63	24
			49	32.7
		F	54	29.4
OW/OB-NF		F	52	24.2
			51	28
			60	31.2
			51	31.9
			43	34.1

		M	50	31.8
			52	31.2
			59	28.7
L-NF		F	37	20.8
			33	24.3
		M	20	23.7
			45	25.1
			46	20.1
L-HF	ICM	M	48	19.7
			25	22.1
			58	22.7
	DCM	F	44	20.7
		M	57	23.9
			34	19.9
			46	21.8

Online References

1. Westermark P, Engström U, Johnson KH, Westermark GT, Betsholtz C. Islet amyloid polypeptide: pinpointing amino acid residues linked to amyloid fibril formation. *Proc. Natl. Acad. Sci. USA*. 1990;87:5036-5040.
2. Matveyenko AV, Butler PC. Islet amyloid polypeptide (IAPP) transgenic rodents as models for Type 2 Diabetes. *ILAR Journal*, 2006;47:225-233.
3. Matveyenko AV, Butler PC. β-cell deficit due to increased apoptosis in the human islet amyloid polypeptide transgenic (HIP) rat recapitulates the metabolic defects present in type-2 diabetes. *Diabetes* 2006;55:2106-2114.
4. Cummings BP, Digitale EK, Stanhope KL, Graham JL, Baskin DG, Reed BJ, Sweet IR, Griffen SC, Havel PJ. Development and characterization of a novel rat model of type 2 diabetes mellitus: the UC Davis type 2 diabetes mellitus UCD-T2DM rat. *Am. J. Physiol. Regul. Integr. Comp. Physiol.* 2008;295:R1782-1793.
5. Cummings BP, Stanhope KL, Graham JL, Baskin DG, Griffen SC, Nilsson C, Sams A, Knudsen LB, Raun K, Havel PJ. Chronic administration of the glucagon-like peptide-1 analog, liraglutide, delays the onset of diabetes and lowers triglycerides in UCD-T2DM rats. *Diabetes* 2010;59:2653-2661.
6. Cummings BP, Strader AD, Stanhope KL, Graham JL, Lee J, Raybould HE, Baskin DG, Havel PJ. Ileal interposition surgery improves glucose and lipid metabolism and delays diabetes onset in the UCD-T2DM rat. *Gastroenterology* 2010;138:2437-2446.
7. Cummings BP, Bettaieb A, Graham JL, Stanhope KL, Dill R, Morton GJ, Haj FG, Havel PJ. Subcutaneous administration of leptin normalizes fasting plasma glucose in obese type 2 diabetic UCD-T2DM rats. *Proc Natl Acad Sci U S A* 2011;108:14670-1475.
8. Despa S, Bers DM. Functional analysis of Na/K-ATPase isoform distribution in rat ventricular myocytes. *Am J Physiol - Cell Physiol* 2007;293:C321-C327.
9. Lin L, Kim SC, Wang Y, Gupta S, Davis B, Simon SI, Torre-Amione G, Knowlton AA. HSP60 in heart failure: abnormal distribution and role in cardiac myocyte apoptosis. *Am. J. Physiol. Heart Circ. Physiol.* 2007;293:H2238-H2247.
10. Walton JH, Berry RS, Despa F, Amyloid oligomer formation probed by water proton magnetic resonance spectroscopy. *Biophys. J.* 2010;100:2302-2308.